Osteichthyan-like cranial conditions in an Early Devonian stem gnathostome

Sam Giles[1], Matt Friedman[1], Martin D. Brazeau[2,3]*

[1]Department of Earth Sciences, University of Oxford, South Parks Road, Oxford, OX1 3AN, UK.

[2]Naturalis Biodiversity Center, P.O. Box 9517, 2300 RA Leiden, The Netherlands.

[3]Department of Life Sciences, Imperial College London, Silwood Park Campus, Buckhurst Road, Ascot, SL5 7PY, UK.

*Corresponding author. E-mail: m.brazeau@imperial.ac.uk

[First paragraph: ca. 293 words]

The phylogeny of Silurian and Devonian (443-358 million years ago [Ma]) fishes remains the foremost problem in the study of the origin of modern gnathostomes (jawed vertebrates). A central question concerns the morphology of the last common ancestor of living jawed vertebrates, with competing hypotheses advancing either a chondrichthyan-[1-3] or osteichthyan-like[4,5] model. Here we present *Janusiscus schultzei* gen. et sp. nov., an Early Devonian (ca. 415 Ma) gnathostome from Siberia previously interpreted as a ray-finned fish[6], which provides important new information about cranial anatomy near the last common ancestor of

chondrichthyans and osteichthyans. The skull roof of *Janusiscus* resembles that of early osteichthyans, with large plates bearing vermiform ridges and partially enclosed sensory canals. High-resolution computed tomography reveals a braincase bearing characters typically associated with either chondrichthyans (large hypophyseal opening accommodating the internal carotid arteries) or osteichthyans (facial nerve exiting through jugular canal, endolymphatic ducts exiting posterior to the skull roof) and lacking a ventral cranial fissure, the presence of which is considered a derived feature of crown gnathostomes[7,8]. A conjunction of well-developed cranial processes in *Janusiscus* helps unify the comparative anatomy of early jawed vertebrate neurocrania, suggesting primary homologies in 'placoderms', osteichthyans and chondrichthyans. Phylogenetic analysis further supports the chondrichthyan affinities of 'acanthodians', and places *Janusiscus* and the enigmatic *Ramirosuarezia*[9] in a polytomy with crown gnathostomes. The close correspondence between the skull roof of *Janusiscus* and that of osteichthyans strongly suggests an extensive dermal skeleton was present in the last common ancestor of jawed vertebrates[4], but ambiguities arise from uncertainties in the anatomy of *Ramirosuarezia*. The unexpected contrast between endoskeletal structure in *Janusiscus* and its superficially osteichthyan-like dermal skeleton highlights the potential significance of other incompletely known Siluro-Devonian 'bony fishes' for reconstructing patterns of trait evolution near the origin of modern gnathostomes.

[Main text: 1536 words]

Gnathostomata (Gegenbaur 1878)

***Janusiscus schultzei* gen. et sp. nov**

Diagnosis. A jawed vertebrate characterised by a rectilinear pattern of skull roof bones bearing vermiform ridges but lacking endochondral bone, a ventral cranial fissure and vestibular fontanelles. Skull roof differs from those attributed to the type species of *Dialipina* (*Dialipina salgueiroensis*)[10] in having postparietals longer than parietals, and parietals lacking anterolateral extensions. Principal autapomorphy of *Janusiscus* is a boundary between parietals and postparietals that slopes posteriorly towards the midline, with the postparietals forming distinct anterolateral processes (as per the original description[6]). Braincase with broad otic region, and narrow sphenoid pierced by large hypophyseal opening and bearing pronounced ventrolateral ridges.

Etymology. Generic name refers to double-sided nature of the specimen, with an osteichthyan-like dorsal skull roof, but a braincase that displays an array of plesiomorphic gnathostome characters (Latin *Ianus*, the god of doorways and transitions, often depicted as having two faces; [p]*iscis*, fish). Specific name in honour of Hans-Peter Schultze (University of Kansas), who first described these specimens[6].

Holotype. GIT (Institute of Geology, Talinn, Estonia) 496-6 (Pi.1384), skull roof and braincase, both missing anterior region, (Fig. 1; Extended Data Figure 1a,3).

Locality and horizon. Lower member, Kureika Formation, Sida River, Kotui Basin, Siberia. The presence of the zone fossil *Rhinopteraspis crouchi* in a lateral equivalent of the Kureika Formation[11] restricts the age of this deposit to middle Lochkovian (ca. 415 Ma[12]) . This is consistent with evidence drawn from other biostratigraphic markers (Supplementary Information file).

Remarks and referred material. We refer a second, more complete skull roof (GIT 496-7 [Pi. 1383]; Extended Data Figure 1c) from the type locality to *Janusiscus*. Rhombic scales lacking clear dorsal pegs are also known from this deposit (GIT 496-8 – 496-16; Extended Data Figure 2a-c), but cannot be definitively associated with cranial material. All of these remains were previously attributed[6] to *Dialipina markae*, the type of which is an isolated scale bearing a modest peg from the Lower Devonian of Kotelny Island, New Siberian Islands[13] (ca. 1500 km from the Sida River site).

Description. The skull roof comprises paired parietals and postparietals, and a median pineal plate (Fig. 1a, Extended Data Figure 1). The anterior part of the skull roof, including the pineal, is not preserved in the holotype. All bones are ornamented with vermiform ridges, although the histological structure of these ridges is not preserved (Extended Data Figure 2h-j). The supraorbital sensory canals extend across the parietals and postparietals in open grooves but are enclosed in bony tubes posteriorly (Extended Data Figure 3). The postparietal bears a middle pit-line behind the termination of the

supraorbital canal. The pattern of dermal ornament in the posterior part of the skull suggests the presence of posteriorly placed pitlines (as in '*Ligulalepis*'[14]).

High-resolution CT scanning of GIT 496-6 reveals a nearly complete perichondrally ossified neurocranium, lacking evidence of endochondral mineralization (Fig. 1; Extended Data Figures 4,5). The incompletely preserved ethmoid is comineralized with the remainder of the braincase. The basisphenoid is elongate and mediolaterally narrow, resembling conditions in *Acanthodes*[3] and osteichthyans[15,16]. The basisphenoid bears a large, diamond-shaped hypophysial opening but no evidence of a parasphenoid. Subcranial ridges like those of *Doliodus*[17] define the lateral margins of the basisphenoid and extend posteriorly to the otic region (Extended Data Figure 5). The modest basipterygoid processes emerge as slight flanges posterior to the level of the hypophysis. Like 'placoderms'[18,19] and many chondrichthyans[20,21], *Janusiscus* lacks a ventral cranial fissure. The gently concave parachordal region tapers toward the occiput where its edges form ventral cristae that border grooves for the lateral dorsal aortae. The occipital margin bears a notch that is aligned with a midline thickening of the parachordal surface.

Two prominent transverse processes are present (Fig. 1a,b). The postorbital process defines the rear margin of the orbit. The passage of the jugular vein through the postorbital process is unclear. It bears a ventral notch and a posterodorsal opening, either of which may have accommodated the jugular vein. The transverse otic process is separated from the postorbital process by a wide postorbital fossa. This process terminates distally in a single hyomandibular facet, and is pierced by the jugular canal.

An enclosed canal for the hyomandibular branch of the facial nerve intersects that of the jugular (Extended Data Figure 3).

The suborbital and supraorbital shelves are well developed. The orbital wall is interrupted by a large eyestalk attachment with a raised posteroventral rim (Fig. 1c,d and Extended Data Figure 6c-e). The optic nerve exited through a foramen anterior to the eyestalk area. Foramina for the oculomotor, profundus and abducens nerves, along with associated myodomes, are present along an arc in the rear of the orbit (Extended Data Figure 6).

The otic capsules are broad, protruding well beyond the lateral margins of the basicranium (Extended Data Figure 3). Paired endolymphatic ducts emerge from the roof of the braincase immediately posterior to the skull roof (Extended Data Figure 2,3). Vestibular fontanelles are absent, but the condition of the metotic fissure is unclear. The narrow occipital region extends well behind the otic capsules. A mineralized shelf separates the cavum cranii from the notochordal canal (Fig. 1e).

Comparative anatomy. *Janusiscus* presents an unexpected suite of osteichthyan, chondrichthyan, and generalised gnathostome traits. A rectilinear pattern of skull roof bones bearing vermiform ornament, partially buried sensory canals, endolymphatic ducts opening posterior to the dermal skull roof, and the exit of the hyomandibular branch of the facial nerve into the jugular canal are features typically associated with osteichthyans[22,23]. However, the combination of a flat-based braincase, weakly developed basipterygoid processes, absence of vestibular fontanelles, and absence of a ventral cranial fissure are inconsistent with *Janusiscus* as a crown-group osteichthyan and

therefore also with the original actinopterygian diagnosis[6] and its current use as a fossil calibration in ray-finned fish molecular clocks[24].

Janusiscus possesses some chondrichthyan-like features, including the absence of paired openings for the internal carotids, a condition also shared with *Acanthodes*. Instead, the internal carotids entered the braincase through the large hypophyseal opening. The subcranial ridges flanking the ventrolateral angle of the braincase in *Janusiscus* strongly resemble those in the early chondrichthyan *Doliodus*[17].

At least four pairs of transverse cranial processes are present on the braincases of some early gnathostomes (Supplementary Information file; Fig. 2, Extended Data Figure 7). The prominent transverse walls in *Janusiscus* allow us to address the primary homology of the anterior two processes. Comparison with crown group osteichthyans and placoderms reveals that the so-called 'supraorbital process' of arthrodires corresponds to the postorbital process of crown group gnathostomes (including the postorbital pila of sarcopterygians[25]) and the postorbital pila of *Entelognathus*[4]. The 'anterior postorbital process' of placoderms can be homologized with the transverse otic process of osteichthyans. The transverse otic process appears substantially reduced or lost in *Acanthodes*[3] and the earliest chondrichthyans[7,8,16], though it may correspond to the prominent lateral otic process of later chondrichthyans such as *Orthacanthus* and *Tamiobatis* (Extended Data Figure 7). This further corroborates recent anatomical reinterpretations of *Acanthodes*[3] and its placement in the chondrichthyan total group[4,5].

Phylogenetic analysis. Phylogenetic analysis recovers *Janusiscus* in a polytomy with *Ramirosuarezia* and the gnathostome crown. This corroborates our removal of the

Siberian material from the genus *Dialipina*, which we recover as a stem osteichthyan[2-5]. Our result provides the first analytical placement for the enigmatic *Ramirosuarezia*, which has previously been compared with 'placoderm'-grade stem gnathostomes[9,26] and holocephalan chondrichthyans[9].

While our analysis favours the stem gnathostome hypothesis for *Janusiscus*, we consider stem chondrichthyan and stem osteichthyan placements reasonable alternatives: both require only one additional step. Placement of *Janusiscus* on the chondrichthyan stem may seem provocative, but the hypothesis of micromery as a derived chondrichthyan trait predicts macromeric stem chondrichthyans. While there is ambiguity in the position of *Janusiscus* relative to the three branches incident to the gnathostome crown node, we reject an actinopterygian interpretation[6], which requires 7 additional steps.

The new anatomical details of *Janusiscus* and our phylogenetic result corroborate the recently revived hypothesis that 'acanthodians' are total group chondrichthyans. The osteichthyan-like skull roof of *Janusiscus* strongly implies that the continuous dermal armour common to 'placoderms' and bony fishes is a gnathostome symplesiomorphy[4,5]. However, uncertainty about conditions of the exoskeleton in *Ramirosuarezia* precludes more definitive statements about the nature of the dermal skeleton in the earliest crown gnathostomes. We find that chondrichthyans (including all 'acanthodians') and osteichthyans are united to the exclusion of *Janusiscus* by the presence of a ventral cranial fissure separating the otic and sphenoid regions of the braincase (Fig. 3). The revised comparative framework for gnathostome braincases provided by *Janusiscus*

highlights substantial neurocranial modifications uniting total-group chondrichthyans (e.g. loss of jugular vein canal in the otic region; hyomandibular articulation at level of posterior semicircular canal, Fig. 3)[23], while casting doubt on the validity of some supposed osteichthyan synapomorphies (e.g. exit of the hyomandibular branch of the facial nerve through the jugular canal, Extended Data Figure 3).

This work reinforces an emerging consensus for osteichthyan-like anatomical conditions in stem gnathostomes and possibly the last common ancestor of crown-group gnathostomes[4,5]. The recognition that many features of the bony fish dermal skeleton might be general traits of modern jawed vertebrates highlights the need to revisit the roughly half-dozen supposed stem osteichthyans known only from isolated dermal fragments[22,27,28]. Significantly, our results suggest the plausibility of alternative placements of some of these taxa as either stem gnathostomes or even stem chondrichthyans.

References

1. Miles, R. S. in *Interrelationships of Fishes* (eds Greenwood, P. H., Miles, R. S. & Patterson, C.) 63–103 (Academic, 1973).
2. Brazeau, M. D. The braincase and jaws of a Devonian ‘acanthodian’ and modern gnathostome origins. *Nature* **457,** 305–308 (2009).
3. Davis, S. P., Finarelli, J. A. & Coates, M. I. Acanthodes and shark-like conditions in the last common ancestor of modern gnathostomes. *Nature* **486,** 247–250 (2012).

4. Zhu, M. *et al.* A Silurian placoderm with osteichthyan-like marginal jaw bones. *Nature* **502**, 188–193 (2013).

5. Dupret, V., Sanchez, S., Goujet, D., Tafforeau, P. & Ahlberg, P. E. A primitive placoderm sheds light on the origin of the jawed vertebrate face. *Nature* **507,** 500–503 (2014).

6. Schultze, H.-P. in Fossil Fishes as Living Animals (ed. Mark-Kurik, E.) 233–242 (Academy of Sciences of Estonia, 1992).

7. Maisey, J. G. in *Major Events in Early Vertebrate Evolution* (ed. Ahlberg, P. E.) 263–288 (Taylor & Francis, 2001).

8. Maisey, J. G. & Anderson, M. E. A primitive chondrichthyan braincase from the Early Devonian of South Africa. *J. Vertebr. Paleontol.* **21,** 702–713 (2001).

9. Pradel, A., Maisey, J. G., Tafforeau, P. & Janvier, P. An enigmatic gnathostome vertebrate skull from the Middle Devonian of Bolivia. *Acta Zoologica* 90, 123–133 (2009).

10. Schultze, H.-P & Cumbaa, S. L. in *Major Events in Early Vertebrate Evolution* (ed. Ahlberg, P. E.) 315–332 (Taylor & Francis, 2001).

11. Blieck, A. & Janvier. in *Palaeozoic Vertebrate Biostratigraphy and Biogeography* (ed. Long, J. A.) 87–103 (Belhaven, 1993).

12. Gradstein, F. M., Ogg, J. G., Schmitz, M. & Ogg, G. The Geologic Time Scale 2012 (Elsevier, 2012).

13. Schultze, H.-P. Ausgangsform und Entwicklung der rhombischen Schuppen der Osteichthyes (Pisces). *Paläontol. Z.* **51,** 152–168 (1977).

14. Basden, A. M. & Young, G. C. A primitive actinopterygian neurocranium from

the Early Devonian of Southeastern Australia. *J. Vertebr. Paleontol.* **21,** 754–766 (2001).

15. Jarvik, E. *Basic Structure and Evolution of Vertebrates* (Academic, 1980).

16. Gardiner, B. G. The relationships of the palaeoniscid fishes, a review based on new specimens of *Mimia* and *Moythomasia* from the Upper Devonian of western Australia. *Bull. Br. Mus. Nat. Hist.* **37**, 173–428 (1984).

17. Maisey, J. G., Miller, R. & Turner, S. The braincase of the chondrichthyan *Doliodus* from the Lower Devonian Campbellton Formation of New Brunswick, Canada. *Acta Zoologica* **90** (suppl. 1), 109–122 (2009).

18. Stensiö, E. Anatomical studies on the arthrodiran head, part I. *Kungl. Svensk. Vetenskakad. Handl.* **9**, 1–419 (1963).

19. Goujet, D. *Les poissons placodermes du Spitsberg*. (Cahiers de Paléontologie, Section Vertébrés, Centre National de la Recherche Scientifique, 1984).

20. Schaeffer, B. The xenacanth shark neurocranium, with comments on elasmobranch monophyly. *Bull. Am. Mus. Nat. Hist.* **169**, 1–66 (1981).

21. Maisey, J. G. Braincase of the Upper Devonian shark *Cladodoides wildungensis* (Chondrichthyes, Elasmobranchii), with observations on the braincase in early chondrichthyans. *Bull. Am. Mus. Nat. Hist.* **288**, 1–103 (2005).

22. Friedman, M. & Brazeau, M. D. A reappraisal of the origin and basal radiation of the Osteichthyes. *J. Vertebr. Paleontol.* **30,** 36–56 (2010).

23. Brazeau, M. D. & Friedman, M. The characters of Palaeozoic jawed vertebrates. *Zool. J. Linn. Soc.* **170**, 779–821 (2014).

24. Broughton, R. B.-R., Li, C., Arratia, G. & Ortí, G., Richard E Broughton, R.

Multi-locus phylogenetic analysis reveals the pattern and tempo of bony fish evolution. *PLoS Currents* **5,** (2013).

25. Yu, X-B. A new porolepiform-like fish, *Psarolepis romeri*, gen. et sp. nov. (Sarcopterygii, Osteichthyes) from the Lower Devonian of Yunnan, China. *J. Vertebr. Paleontol.* **18**, 261–274 (1998).

26. Anderson, P. S. L., Friedman, M., Brazeau, M. D. & Rayfield, E. J. Initial radiation of jaws demonstrated stability despite faunal and environmental change. *Nature* **476**, 206–209 (2011).

27. Botella, H., Blom, H., Dorka, M., Ahlberg, P. E. & Janvier, P. Jaws and teeth of the earliest bony fishes. *Nature* **448,** 583–586 (2007).

28. Cunningham, J. A., Rucklin, M., Blom, H., Botella, H. & Donoghue, P. C. J. Testing models of dental development in the earliest bony vertebrates, *Andreolepis* and *Lophosteus*. *Biol. Lett.* **8**, 833–837 (2012).

29. Young, G. C. New information on the structure and relationships of *Buchanosteus* (Placodermi: Euarthrodira) from the Early Devonian of New South Wales. *Zool. J. Linn. Soc.* **66**, 309–352 (1979).

Supplementary Information is linked to the online version of the paper at www.nature.com/nature.

Acknowledgements We thank U. Toom for access to material, E. Mark-Kurik for discussions on stratigraphy and specimen provenance, W. Renema and R. Garwood for assistance with scanning. This work was supported by NERC Cohort NE/J500045/1 grant

to S.G., the Philip Leverhulme Prize and John Fell Fund, both to M.F., and the European Research Council under the European Union's Seventh Framework Programme (FP/2007-2013) / ERC Grant Agreement number 311092 to M.D.B.

Author Contributions The project was conceived by M.D.B. and M.F. Computed tomography scanning was conducted by M.F. and M.D.B. S.G. generated the computed tomography renderings. Main text figures and illustrations were produced by M.D.B. and S.G. with input from M.F. All authors participated in the generation of phylogenetic data. M.D.B. conducted the phylogenetic analyses. All authors participated in the interpretation of the specimen data and writing the manuscript, and generating supplementary text and illustrations.

Author Information The LSIDs urn:lsid:zoobank.org:pub:CFD16449-8A34-4401-9E01-289EA91C2C77 (article), urn:lsid:zoobank.org:act:652A7405-164B-4D58-B5AF-F21EDF552303 (genus), and urn:lsid:zoobank.org:act:3BD31DC4-11E1-4510-A185-B295CC626C07 (species) have been deposited in ZooBank. Reprints and permissions information is available at www.nature.com/reprints. The authors declare no competing financial interests. Correspondence and requests for materials should be addressed to m.brazeau@imperial.ac.uk.

Figure Legends

Figure 1 | The skull of *Janusiscus schultzei* gen. et sp. nov. based on high-resolution computed tomography of GIT 496-6 (Pi.1384). a, Dorsal (left) and ventral views. **b,**

Interpretive drawing of ventral view. **c,** Right lateral view. **d,** Interpretive drawing of right lateral view. **e,** Posterior view. Scale bar, 5 mm.

Figure 2 | Comparative braincase morphology of selected Palaeozoic gnathostomes. Braincases are aligned on the hypophyseal opening, the position of which is indicated by the horizontal pink line. The path of the major cranial blood vessels is shown in red, with inferred paths represented by dotted lines. Character distributions reject the homology of craniospinal processes in 'placoderms' and actinopterygians. Illustrations are redrawn from refs 4, 16-17, and 29.

Figure 3 | Summary result of phylogenetic analyses. Some clades collapsed or omitted for simplicity. Shaded disks represent ranges of bootstrap support, numbers at nodes are decay indices. Full cladograms provided in Extended Data Figures 8-9 and Supplementary Information 1.

Methods

X-ray computed microtomography. GIT 496-6 was scanned using a SkyScan1172 combining two vertically overlapping scan series of 7200 projections with an energy of 100 kV and 100µA and 4.75 seconds exposure. Scan data were analysed using Mimics (biomedical.materialise.com/mimics; Materialise, Leuven, Belgium). After segmenting, surface meshes were exported into and imaged in Blender (blender.org; Stitching Blender Foundation, Amsterdam, the Netherlands).

Phylogenetic analysis.

Phylogenetic analysis was performed in PAUP* 4.0b10[30] using a dataset with 236 characters (three of which were ordered: 64, 126 and 166) and 78 taxa. The dataset is based on ref 3. In addition to a number of coding changes, one highly incomplete taxon (*Rhadinacanthus*) and four characters were deleted from the matrix of Davis et al. (ref. 3); full justification for excluded characters is given in the character list. Additional characters were taken from a variety of sources, and are referenced in the character list. In addition to *Janusiscus* and taxa carried forward from Davis et al., we added 18 taxa spanning most taxonomic assemblages of Palaeozoic gnathostomes. In the case of *Janusiscus*, we coded as uncertain any characters relating to scale morphology and histology; the Siberian scales originally referred to *D. markae* were not directly associated with the braincase, and their affinity is thus uncertain (for further details, see Supplementary Information file). We follow a similar convention with the braincase attributed to '*Ligulalepis*', and hence scale and histology characters are coded as uncertain. We assessed taxonomic equivalence (sensu Wilkinson[31]) using the software package TAXEQ3[32]. No taxa showed non-unique combinations of character states that would permit safe taxonomic reduction, so analyses were executed with a complete taxon set. Although several taxa are highly incomplete, we followed the recommendations of Wiens[33,34] by maximizing the absolute number of characters instead of deleting incomplete or fragmentary taxa.

We conducted a heuristic search using 1000 random addition sequence replicates, holding 5 trees at each step, and the tree bisection and reconnection (TBR) strategy. Maxtrees was

set to automatically increase by 100. To prevent outgroup taxa from moving to the ingroup or collapsing of the ingroup node, we employed a rooted constraint tree, keeping only trees consistent with the following general topology: (Galeaspida(Osteostraci(Ingroup))).

Bootstrap values were calculated using 15000 replicates of a heuristic search using random addition sequence, 10 replicates, holding 5 trees at each step, using the TBR strategy. To speed up the search, we set a limit of 20 million rearrangements per addition sequence replicate (options: rearrlimit=20000000 limitperrep=yes in the hsearch command in PAUP*).

Node decay values (i.e. Bremer support) were calculated manually using 20 random addition sequence replicates of a heuristic search, rearrlimit=200000000, limitperrep=yes, and by incrementing the KEEP score by 1 over the length of the shortest tree found. Nodes retained in the strict consensus tree had their decay index incremented by one.

We conducted a set of further searches using the protocols outlined above with the following modifications. First, we conducted an equally weighted analysis minus *Janusiscus* to assess whether inferred patterns of relationships among early gnathostomes were robust to exclusion of the genus. To test whether the tree topology was sensitive to the removal of random taxa, we conducted an additional five searches each following the removal of a randomly selected terminal. Random selection was conducted using Microsoft Excel's RANDBETWEEN function with parameters set to 3 and 78 (we

excepted the outgroup from random pruning) and used the first five results obtained to draw taxa from the list following their order in the Nexus file. To speed up these searches, we used rearrlimit=10000000 and limitperrep=yes. Finally, we reweighted all characters by their retention indices in the shortest trees recovered by our initial analysis that applied equal character weights.

Phylogenetic Results

The phylogenetic search resulted in 522936 trees of 639 steps. A summary strict consensus tree with some clades omitted or collapsed is shown in Fig. 4 in the main text. The complete result is shown in Extended Data Figure 8a. The Adams consensus tree is shown in Extended Data Figure 8b. All unambiguous character state transformations are shown in Supplementary Information 1. A summary strict consensus tree of an analysis of the dataset with characters reweighted by retention index is shown in Extended Data Figure 9a. It preserves all major branching patterns found in the analysis of equally weighted characters, but shows greater resolution within some clades.

Inferred interrelationships are not changed when *Janusiscus* is removed from the analysis (Extended Data Figure 9b), as its influence on how cranial processes are recognized and coded pervades significant parts of the dataset. The removal of an additional five taxa at random (*Cladoselache*, *Tristychius*, *Acanthodes*, *Kentuckia*, *Lupopsyrus*) each had no significant impact on the overall tree topology, excepting differences in the degree of resolution.

The overall large number of trees results in polychotomous branchings primarily concentrated in the chondrichthyan stem compounded with a smaller number of polychotomous branchings in the gnathostome and osteichthyan stems. The Adams consensus shows two principal branching patterns that are consistent within the results. One is a clade of stem chondrichthyans comprising acanthodiforms, ischnacanthids, some diplacanthids, as well as *Latviacanthus* and *Euthacanthus*. The other branching consisted of most *Climatius*-like taxa and conventionally defined chondrichthyans (including the crown group).

Support for key nodes is summarized in Fig. 4, with full details given Extended Data Figure 8a. Unsurprisingly, most are quite low. The highest values are found within well-studied groups (e.g. sarcopterygians and actinopterygians) or associated with clades with numerous specialisations (e.g. holocephalans, bothriolepidid antiarchs). A decay index of 2 and a bootstrap support of 68% are recovered for the clade comprising all chondrichthyans and acanthodians. A decay index greater than 1 is consistent with the very long branch subtending this clade (Supplementary Information 1). The low bootstrap value might be explained by the fact that more than half of the transformations along this branch are homoplasious and have a consistency index of 0.5 or less. In spite of this, the branch is supported by five invariant, unambiguous synapomorphies (see Supplementary Information 1).

Methods References

30. Swofford, D. L. *PAUP*: Phylogenetic analysis using parsimony (* and other methods). version v. 4.0b 10* (Sinauer Associates, 2003).

31. Wilkinson, M. Coping with missing entries in phylogenetic inference using parsimony. *Syst. Biol.* **44**, 501–514 (1995).

32. Wikinson, M. TAXEQ3: software and documentation (Department of Zoology, Natural History Museum, London, 2001).

33. Wiens, J. J. Missing data, incomplete taxa, and phylogenetic accuracy. *Syst. Biol.*, **52**, 528–538 (2003).

34. Wiens, J. J. Incomplete taxa, incomplete characters, and phylogenetic accuracy: is there a missing data problem? *J. Vertebr. Paleontol.* **23**, 297–319 (2003).

Extended Data Figure Legends

1. Anatomical figures

Extended Data Figure 1 | Dermal skull roofing bones of *Janusiscus* and *Dialipina salgueiroensis*. a, Photograph of the holotype (GIT 496-6 [Pi.1384]). **b,** Original interpretation mofifed from Schultze (1992). Reinterpretation of bones italicized in brackets (where applicable). **c,** Photograph of the referred skull roof (GIT 496-7 [Pi.1383]). **d,** Original interpretation modified from Schultze (1992). **e,** New interpretive drawing of the holotype (GIT 496-6 [Pi.1384]). **f,** New interpretive drawing of the referred skull roof (GIT 496-7 [Pi.1383]). **g,** *Dialipina salgueiroensis*, modified from Schultze and Cumbaa (2001).

Extended Data Figure 2 | Scales attributed to *Dialipina* and SEM images of *Janusiscus schultzei* n. gen. et sp. Scales from the localities of the Kureika Formation along the Sida River, Kotui Basin, Siberia, previously referred to *D. markae*, in: **a,** external view (GIT 496-8 [Pi.1384a]), previously figured by Schultze (1992; Pl.1, Fig.3); **b,** internal view (GIT 496-10 [Pi.1385b]); **c,** external view (GIT 496-16 [Pi.1387]). Gross scale morphology of *D. salgueiroensis* and referred species of *Dialipina*: **d**, holotype of *D. salgueiroensis*, from the Emsian of Canada. Redrawn from Schultze (1977: fig. 3h); **e**, holotype of *D. markae*, from the Lochkovian of the New Siberian Islands. Redrawn from Schultze (1977: fig. 3a); **f**, scale from the

Kureika Formation, Siberia, referred to *D. markae* by Schultze (1992). Photograph of specimen in **a** Modified from Schultze (1992: fig. 4); **g**, new interpretive drawing of scale in **c**. **h,** Broken edge of the skull roof in the holotype (GIT 496-6 [Pi.1383]). The histological structure is not preserved. **i,** The anterior part of the referred skull roof (GIT 496-7). The dermal bone is poorly preserved, with the bone in the centre of each ridge missing. The histological structure is not preserved. **j,** the holotype (GIT 496-6 [Pi.1384]) in dorsal view, showing the endoskeletal supraoccipital crest and openings of the endolymphatic ducts. Images **a**, **b**, and **c** modified slightly from that by Institute of Geology at TUT and licensed by CC 3.0.
http://geokogud.info/git/specimen_image/496/496-8.jpg;
http://geokogud.info/git/specimen_image/496/496-10.jpg;
http://geokogud.info/git/specimen_image/496/496-16.jpg.

Extended Data Figure 3 | Semi-transparent rendering of the skull of *Janusiscus schultzei* gen. et sp. nov. showing osteichthyan-like traits not visible externally. Scale bar, 5 mm.

Extended Data Figure 4 | *Janusiscus* lacks endochondral ossification. a, The actinopterygian *Kentuckia deani* MCZ 5226, tomographs showing extensive and well-developed endochondral ossification in both the sphenoid (top) and otic (bottom) regions. Bright white objects in both panels are voids within spongy endochodral bone that have been diagenetically infilled with dense (likely iron) minerals. **b**, *Janusiscus schultzei* n. gen et sp. nov. GIT 496-6 [Pi.1384], tomographs showing lack of obvious endochondral ossification in either the sphenoid (top) or otic (bottom) regions. There is also no visual indication of endochondral bone in a break across the ethmoid region of this same specimen.

Extended Data Figure 5 | Subcranial ridges in *Janusiscus* and early crown gnathostomes. a, Reconstructed tomographs showing that the thickenings along the lateral margins of the sphenoid region of *Janusiscus* do not represent artefacts of post-mortem compression. **b**, The 'acanthodian' *Ptomacanthus anglicus* NHMUK PV P 24919a, silicone peel of specimen preserved in negative, dusted with ammonium chloride. Portions of the skull other than the neurocranium partially masked for clarity. **c**, The chondrichthyan *Doliodus problematicus* NBMG 10127/1a, reconstruction of neurocranium based on CT data. **d**, *Janusiscus schultzei* n. gen et sp. nov. GIT 496-6 [Pi.1384], reconstruction of neurocranium based on CT data. Red arrows in each panel indicate subcranial ridges.

Extended Data Figure 6 | Orbit anatomy of *Janusiscus schultzei* n. gen. et sp. a, SEM image into left orbit showing endoskeletal bone and surrounding matrix. **b,** Image based on µ-XRCT scan with matrix digitally removed. **c**, Lateral view into right orbit, with matrix digitally removed. **d,** Anterolateral view into right orbit, with matrix digitally removed. **e,** interpretive drawing of the orbit, based on a composite of the left and right orbits of the holotype, (GIT 496-6 [Pi.1384]).

Extended Data Figure 7 | Comparison of transverse processes in the

braincases of early gnathostomes. a, *Macropetalichthys* (redrawn from Stensiö 1969). **b**, *Dicksonosteus* (redrawn from Goujet 1984). **c**, *Buchanosteus* (redrawn from Young 1979). **d**, *Entelognathus* (redrawn from Zhu et al. 2013). **e**, *Jagorina* (redrawn from Stensiö 1969). **f**, *Ramirosuarezia* (redrawn from Pradel et al. 2009). **g**, *Acanthodes* (redrawn from Davis et al. 2012). **h**, *Doliodus* (redrawn from Maisey et al. 2009). **i**, *Cladodoides* (redrawn from Maisey 2005). **j**, *Orthacanthus* (redrawn from Schaeffer 1981). **k**, *Janusiscus*. **l**, '*Ligulalepis*' (redrawn from Basden & Young 2001). **m**, *Mimipiscis* (redrawn from Gardiner 1984). **n**, *Psarolepis* (redrawn from Yu 1998). **o**, *Gogonasus* (redrawn from Long et al. 1997).

2. Cladograms from phylogenetic analyses

Extended Data Figure 8 | a, Strict consensus of the 522936 shortest trees (639 steps) for 78 taxa and 236 equally weighted characters. Digits above nodes indicate Bremer decay indices above 1. Digits below nodes indicate percentage bootstrap support. **b,** Adams consensus tree of the 522936 shortest trees for 78 taxa and 236 equally weighted characters.

Extended Data Figure 9 | a, Strict consensus tree of 216 trees with a score of 452.52565 resulting from analysis of characters reweighted according to retention index. **b,** Strict consensus of the 128395 shortest trees for 77 taxa and 236 equally weighted characters, with *Janusiscus* removed from the dataset.

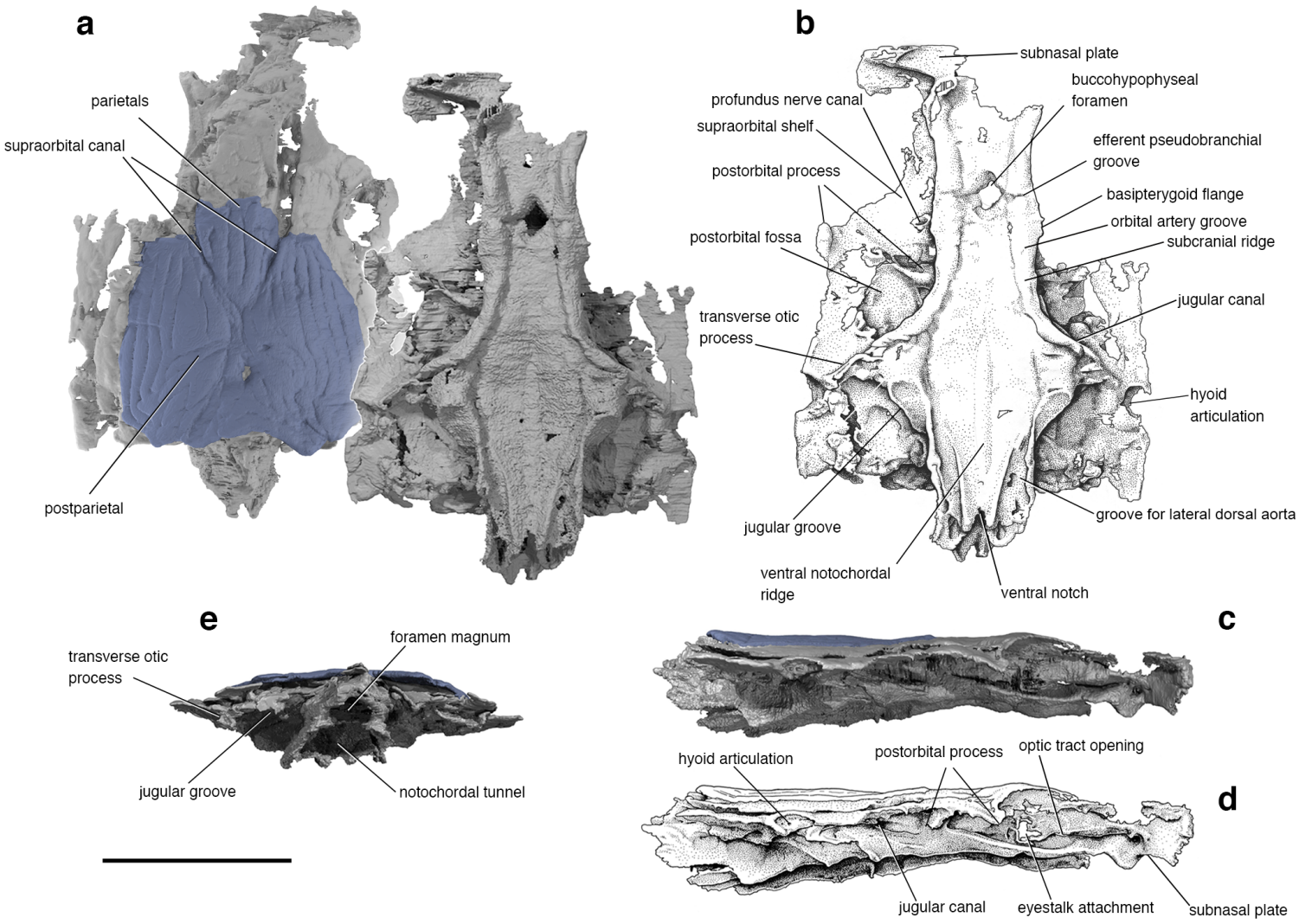
a
parietals
supraorbital canal
postparietal
b
subnasal plate
buccohypophyseal foramen
profundus nerve canal
supraorbital shelf
efferent pseudobranchial groove
postorbital process
basipterygoid flange
orbital artery groove
postorbital fossa
subcranial ridge
jugular canal
transverse otic process
hyoid articulation
groove for lateral dorsal aorta
jugular groove
ventral notochordal ridge
ventral notch
e
foramen magnum
transverse otic process
jugular groove
notochordal tunnel
c
hyoid articulation
postorbital process
optic tract opening
d
jugular canal
eyestalk attachment
subnasal plate

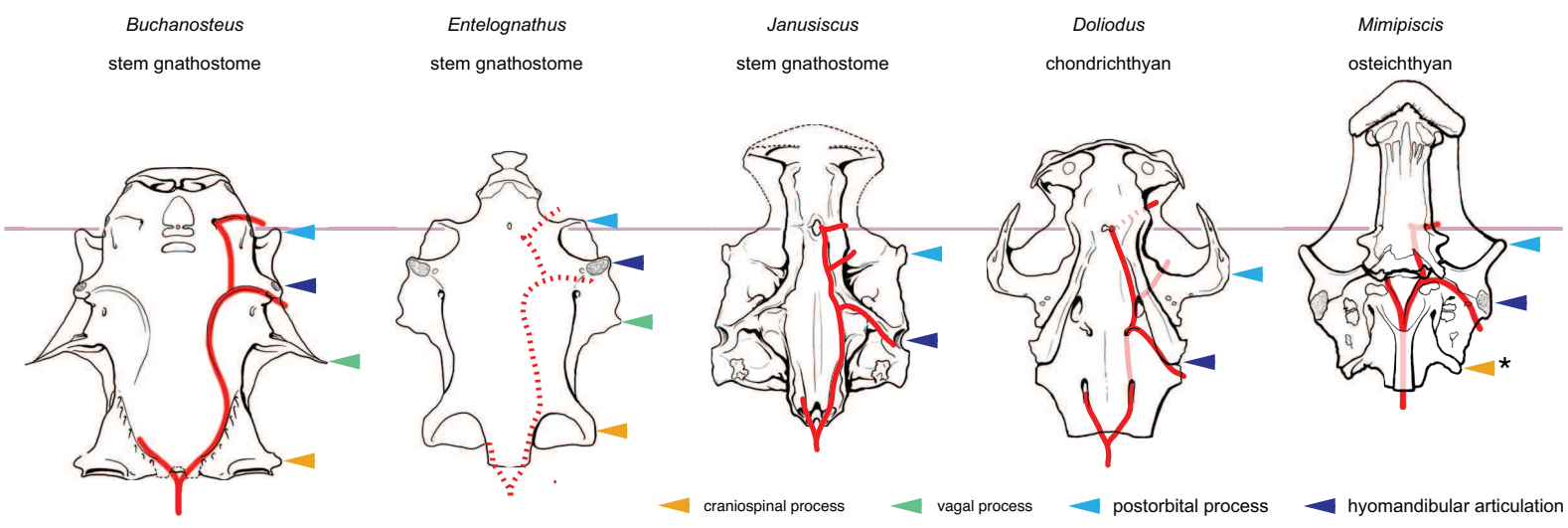
Buchanosteus
stem gnathostome
Entelognathus
stem gnathostome
Janusiscus
stem gnathostome
Doliodus
chondrichthyan
Mimipiscis
osteichthyan
*
craniospinal process
vagal process
postorbital process
hyomandibular articulation

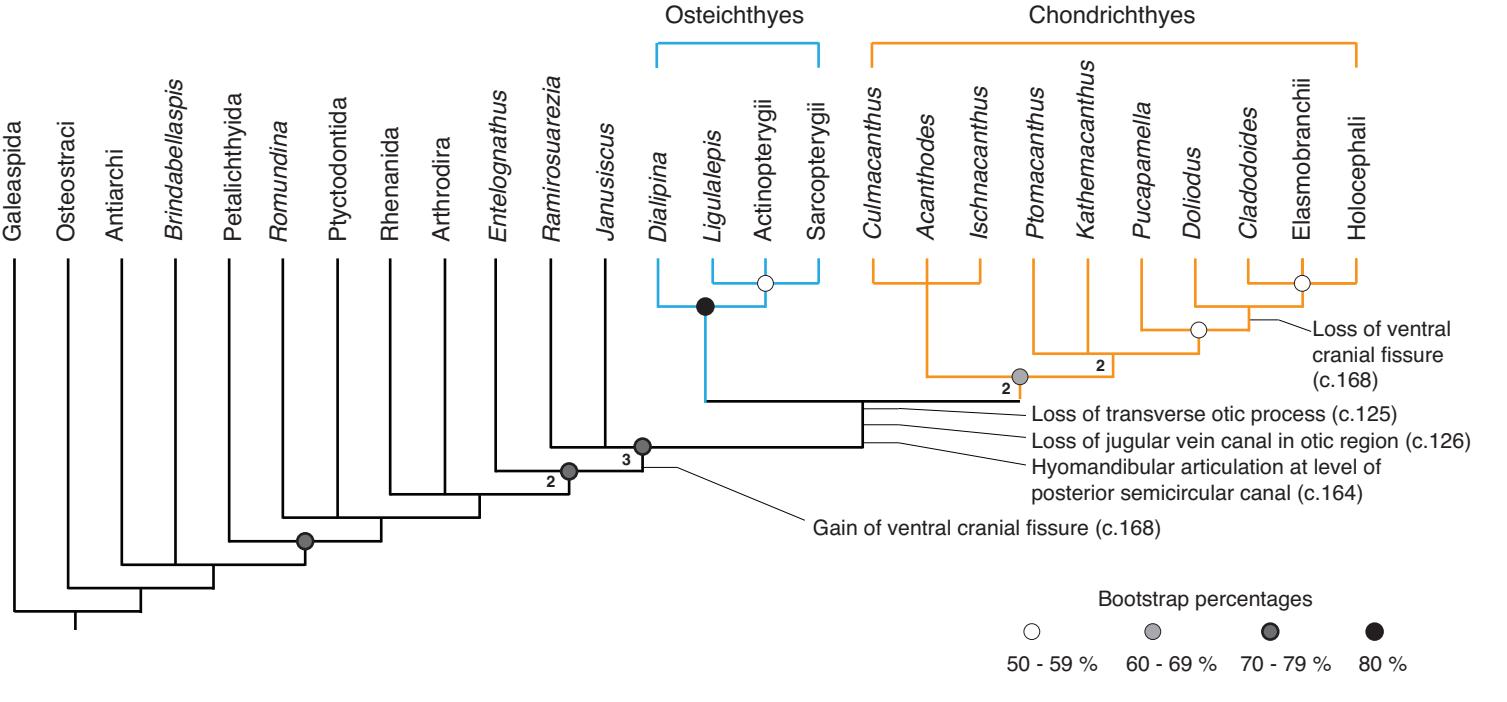
Osteichthyes
Chondrichthyes
Galeaspida
Osteostraci
Antiarchi
Brindabellaspis
Petalichthyida
Romundina
Ptyctodontida
Rhenanida
Arthrodira
Entelognathus
Ramirosuarezia
Janusiscus
Dialipina
Ligulalepis
Actinopterygii
Sarcopterygii
Culmacanthus
Acanthodes
Ischnacanthus
Ptomacanthus
Kathemacanthus
Pucapamella
Doliodus
Cladodoides
Elasmobranchii
Holocephali
2
2
3
2
Loss of ventral cranial fissure (c.168)
Loss of transverse otic process (c.125)
Loss of jugular vein canal in otic region (c.126)
Hyomandibular articulation at level of posterior semicircular canal (c.164)
Gain of ventral cranial fissure (c.168)
Bootstrap percentages
50 - 59 %
60 - 69 %
70 - 79 %
80 %